Environmental Science & Technology

pubs.acs.org/est

Article

Machine Learning-Based Bias-Corrected Future Projections of Ozone Concentrations from a Chemistry-Climate Model

Yiqian Ni, Yang Yang,* Hailong Wang, Pinya Wang, Ke Li, Lei Chen, Jia Zhu, Baojie Li, and Hong Liao

Cite This: *Environ. Sci. Technol.* 2026, 60, 3135−3147

Read Online

ACCESS | Metrics & More | Article Recommendations | Supporting Information

ABSTRACT: Reliable projections of future surface ozone are crucial for air quality management and health risk assessment. However, potential biases in spatial distribution, magnitude, and trends in ozone simulated by global chemistry-climate models limit their applicability in regional evaluations. In this study, LightGBM, a machine learning (ML) algorithm, is applied to correct biases in CESM2-simulated ozone over China, the United States, and Europe and to calibrate future projections under two Shared Socioeconomic Pathways (SSP1−2.6 and SSP5−8.5) from 2020 to 2060. The ML-based correction significantly improves spatial distribution and reduces bias by 40 to 60%, also reversing the potentially incorrect trend under SSP1−2.6 in eastern China. When the ML-based correction is applied to CESM2 projections, the warm-season mean ozone shows substantial changes from 2020 to 2060. Under SSP1−2.6, corrected ozone decreases by 13.5, 17.9, and 13.7 $\mu g/m^3$ in China, the United States, and Europe, respectively. In contrast, under SSP5−8.5, ozone increases over the same period by 9.4, 2.0, and 5.2 $\mu g/m^3$ in these regions. The decomposition analysis shows that anthropogenic emission changes dominate future ozone trends, while a strong climate penalty occurs in polluted eastern China and climate benefits are found in western China, the United States, and Europe under SSP5−8.5. These findings demonstrate the value of combining ML with chemistry-climate models to produce more accurate air quality projections, indicating more effective and region-specific environmental protection strategies.

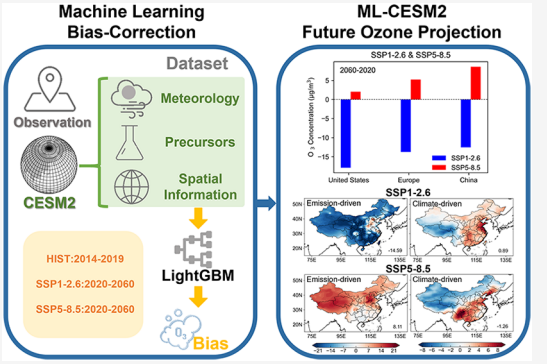

KEYWORDS: *ozone, machine learning, future projection, bias correction*

1. INTRODUCTION

Tropospheric ozone is an atmospheric constituent that contributes to air pollution when its concentration exceeds certain thresholds. The Tropospheric Ozone Assessment Report (TOAR) shows that the highest ozone concentrations are typically observed in the midlatitudes of the Northern Hemisphere.[1,2] Elevated ozone levels in these regions are strongly associated with anthropogenic activities and energy consumption, which result in substantial emissions of ozone precursors.[3]

Many regions have implemented emission control policies.[4−6] Ozone concentrations significantly declined in the United States, increased markedly in East Asia, and remained relatively stable in Europe during 1995−2014.[7,8] These divergent trends can be attributed to region-specific emission control policies, the nonlinear relationship between ozone concentration and its precursor emissions, geographical characteristics, and climate change.[9−13] In China, although the Air Pollution Prevention and Control Action Plan launched in 2013 substantially reduced aerosol concentrations, ozone levels continued to rise, particularly in the densely populated and economically developed eastern provinces.[14−16] Recent studies have also indicated a mitigation trend in ozone pollution in eastern China during 2018−2021, primarily driven by significant reductions in nitrogen oxide (NO_x) emissions.[17]

Ozone pollution is primarily governed by meteorological conditions and emissions of precursors. Recent shifts in meteorological patterns have likely contributed to the aggravation of regional ozone pollution.[18−20] Rising temperatures driven by climate change not only enhance the natural emissions of biogenic ozone precursors but also affect the stratosphere−troposphere exchange and photochemical production of ozone.[21,22] Concurrently, the rising frequency of meteorological stagnation events creates increasingly favorable conditions for the accumulation of atmospheric pollutants.[23−26] Under global warming, these conditions substantially influence ozone concentrations via chemical production, transport, and other pathways, thereby changing the spatiotemporal distribution of ozone pollution. Historical observations have demonstrated that insufficiently coordinated

Received: September 1, 2025
Revised: January 8, 2026
Accepted: January 9, 2026
Published: January 16, 2026

emission reduction strategies, combined with the "climate penalty" effect of global warming, can exacerbate ozone pollution in regions such as Europe, East Asia, and South Asia.[27,28] Xu et al.[29] argued that although climate change could elevate ozone concentrations, pursuing a carbon-neutral emission reduction pathway could lower ozone levels and enable China to achieve the WHO air quality standards. Therefore, precursor emissions and meteorological factors play pivotal roles in modulating ozone concentration variability. Effective ozone pollution mitigation thus necessitates both emission reductions and the development of air quality management strategies that are responsive to climate change.[30]

Atmospheric chemistry models are essential tools for interpreting and forecasting the behavior of atmospheric constituents. However, due to the inherent complexity of atmospheric systems and simplifications in model design, factors such as chemistry, meteorology, emissions, and resolution often cause model predictions to deviate from observed reality.[31] The selection of chemical mechanisms within the model framework also influences the simulated ozone response to precursor emissions, thereby contributing to overall model uncertainty.[32] Some Coupled Model Intercomparison Project Phase 6 (CMIP6) models successfully reproduce the spatial distribution and seasonal variability of tropospheric ozone yet exhibit a tendency to overestimate concentrations in the Northern Hemisphere and underestimate them in the Southern Hemisphere during 1980−2014. These biases are largely attributed to inaccuracies in simulating precursor emissions and chemical processes, as well as uncertainties in tropopause height and stratospheric ozone transport.[33,34] Liu et al.[35] evaluated the UKESM1 model against TOAR observational data and reported that, during 2004−2014, the model underestimated ozone concentrations by 7.2 ppb in winter and overestimated them by 13.4 ppb in summer across regions such as Europe and the United States. He et al.[36] employed the Community Earth System Model (CESM) version 1 to simulate surface ozone concentrations in China and reported an overall overestimation of 15.01 ppb during the warm season (May−September), attributed to the simplified photochemical chemistry and low model resolution of CESM1. Wang et al.[37] compared UKESM1 simulation results with observational data sets and found that during 2005−2019, the model underestimated ozone levels over the North China Plain while overestimated them across western China. These findings highlight that although modern models have the ability to capture global ozone distributions, they still exhibit significant regional biases.

With the rapid advancement of machine learning (ML) techniques, ML-based approaches have become particularly effective at capturing complex nonlinear relationships and spatiotemporal heterogeneity, which are capabilities that traditional statistical methods often lack. By defining the ozone concentrations or the discrepancy between simulated and observed ozone concentrations (i.e., model bias) as the target variable of ML models, and incorporating features pertinent to ozone formation, including spatial and temporal variables, meteorological parameters, anthropogenic emissions, and geographic factors, ML can improve physics-based model predictions and offer pathways to optimize model inputs and outputs.[38] Du et al.[39] conducted a case study in Houston, collecting ground-level ozone data, meteorological information, and traffic data from 2011 to 2020, and validated the performance of the XGBoost algorithm in predicting ozone concentrations with a coefficient of determination (R^2) of 0.78 between the ML prediction and observation. Vairo et al.[40] trained a LightGBM model using meteorological data, ozone measurements from three urban areas, and time variables to forecast ozone concentration in Genoa's (Italy) urban area, achieving excellent predictive power of the ML method. Bertrand et al.[41] enhanced the accuracy of 1-day short-term European air quality forecasts through constructing random forest, gradient boosting, standard, and regularized multilinear models trained with observational data from 1535 European monitoring stations, Copernicus Atmosphere Monitoring Service ensemble forecast data, and meteorological data. Xiong et al.[42] took the model-simulated deviation relative to observations as the target variable and employed the Random Forest algorithm to construct a bias-correction model trained with meteorological and pollution data sets, which significantly enhanced the air quality model's performance in predicting China's daily maximum 8-h ozone concentrations. These previous studies have offered valuable insights into using ML techniques to obtain high-quality data and validated their applicability in China, the United States, and Europe. However, such techniques, especially bias-correction techniques, are predominantly applied in retrospective simulations and have yet to be widely adopted for future ozone projections.

This study utilizes the CESM2 model to simulate ozone over the period from 2020 to 2060 under the Shared Socioeconomic Pathways (SSP) 1−2.6 and SSP5−8.5 scenarios, aiming to explore the impact of anthropogenic emissions on future ozone levels and examine how climate changes modulate ozone pollution in the context of global warming.[43,44] To address the potential biases of simulated ozone concentrations in CESM2, an ML technique is introduced to reduce the uncertainties in model projections, thereby enhancing the robustness of future ozone level predictions. Section 2 details the observational data sources, the CESM2 model, the ML approach, and the experimental design. Section 3 presents the model simulation results along with region-specific calibration analyses using the ML approach for China, the United States, and Europe. Section 4 presents a summary of the key findings and limitations.

2. MATERIALS AND METHODS

2.1. Ozone Data from Observations and CMIP6

This study employs a global modeling framework with detailed regional analyses focusing on China, the United States, and Europe. These regions are selected due to their global significance and representativeness of economic activity, industrial development, environmental governance, and climate change responsiveness. In addition, these regions possess well-established environmental monitoring systems and extensive data resources that offer high-quality inputs for scientific analysis. Consequently, these regions have received considerable attention and in-depth analysis in previous studies.[27]

To evaluate the performance of CESM2 model simulations in predicting ozone concentrations, we collect daily surface ozone observations from multiple countries in China, the United States, and Europe during 2014−2020, and quantify model biases by calculating the differences between observations and model outputs. These observational data sets have been extensively used in previous studies investigating global air pollution.[12,45,46] The network is predominantly concentrated in the eastern China regions, with sparser coverage in the west, particularly over the Tibetan Plateau. The monitoring sites in China, the United States, and Europe are primarily located in densely populated and economically active regions, making them

https://doi.org/10.1021/acs.est.5c11992
Environ. Sci. Technol. 2026, 60, 3135−3147

highly representative. Ozone data from CMIP6 models are utilized to characterize the performance of current state-of-the-art global climate models in simulating ozone distributions. Specifically, ozone concentration outputs over 2015−2019 from multiple global climate models under SSP3−7.0 are used in this study, treated as historical model data. Detailed information on the specific CMIP6 models included in this analysis is provided in Table S1.

2.2. Model Configuration and Experimental Design

This study employs CESM2 to simulate atmospheric species using the FCHIST component set. The model configuration incorporates the atmosphere model CAM6 integrated with the complex chemical module, data ocean component, land model CLM5, sea ice model CICE5, river routing model MOSART, land ice model CISM2, and wave model SWAV. CESM2 integrates a 90-species chemical module CAM6-Chem, which includes the MOZART-TS1 chemical mechanism covering both tropospheric and stratospheric chemistry.[47] It also incorporates the Volatility Basis Set (VBS) scheme for secondary organic aerosol formation, enabling more accurate simulation of aerosols and ozone than earlier model versions.[48] The atmosphere model CAM6 employs the horizontal resolution of 0.9° latitude × 1.25° longitude. CAM6 uses a finite-volume dynamical core with 32 vertical levels extending to 3.6 hPa (~40 km).[49,50] Above this model top, CAM6-Chem applies a standard specified-flux upper boundary condition for the chemical species. Within the resolved atmospheric column, stratospheric ozone is simulated interactively by the full gas-phase chemical mechanism.

In this study, we conduct four experiments to quantify future changes in ozone concentrations driven by variations in climate and emissions under the low-emission scenario (SSP1−2.6) and the extreme warming scenario (SSP5−8.5) from 2020 to 2060. These experiments aim to isolate and evaluate the individual and combined impacts of climate change and emission changes on ozone levels. Emissions (EMIs) are obtained from the Coupled Model Intercomparison Project Phase 6 (CMIP6), including anthropogenic and biomass burning emissions of NO_x, volatile organic compounds (VOCs), CO and other species, following the corresponding scenarios (Figure S1).[51−53] Biogenic emissions are simulated interactively using MEGAN v2.1, which depends on meteorological inputs from CLM5, including surface air temperature, photosynthetically active radiation, soil moisture, humidity, canopy temperature, wind speed, and the CO_2 concentration. Because these meteorological fields evolve differently under SSP1−2.6 and SSP5−8.5, the resulting biogenic emissions respond dynamically to the scenario-dependent changes in temperature, radiation, and hydrological conditions.[54] Methane (CH_4) concentrations are derived from CMIP6, varying consistently with the respective scenarios. The climate change in simulations is driven by changes in prescribed sea surface temperatures (SST) and sea ice concentrations (SIC) data, critical factors influencing atmospheric dynamics and climate patterns. Variations in SST/SIC can significantly affect atmospheric processes by altering heat fluxes between the ocean and atmosphere, modifying large-scale circulation systems, and modulating climate phenomena, thereby serving as a key driver of global and regional climate.[55,56] This method significantly reduces time and resource consumption for climate simulation with external forcings, especially when considering the simulation of atmospheric chemistry. The SST/SIC data used in this study are obtained from the multimodel ensemble mean of CMIP6 (Figure S2). By incorporating projected monthly mean SST/SIC data for the period of 2020−2060, this study investigates how SST/SIC-driven climate changes interact with emission pathways to influence future ozone pollution under contrasting scenarios. Four sensitivity experiments are designed as follows:

SSP585_EMI: SST/SIC fixed in 2020 and EMIs under the SSP5−8.5 scenario.

SSP585_ALL: both SST/SIC and EMIs following the SSP5−8.5 pathway.

SSP126_EMI: SST/SIC fixed in 2020 and EMIs under the SSP1−2.6 scenario.

SSP126_ALL: both SST/SIC and EMIs following the SSP1−2.6 pathway.

All simulations are conducted for the period of 2010−2060, with the first 10 years allocated to model spin-up. In this study, the warm season is defined as the period from April to September during which ozone pollution reaches its peak in the Northern Hemisphere. The CESM2 model has undergone extensive evaluation for its capability to simulate tropospheric ozone.[57,58] To further reduce discrepancies between the CESM2 model and ozone observations, one additional simulation is performed for the period 2012−2019, considering the available observations and emission data sets, driven by SST/SIC data obtained from the HadOIBl data set, with the first two years used for model spin-up. To maintain consistency with observations, meteorological fields for this experiment are nudged to MERRA-2 reanalysis.[59]

2.3. Machine Learning

In this study, the Light Gradient Boosting Machine (LightGBM) model is employed to predict the difference between the observed ozone concentrations and CESM2-simulated values. This ML model is selected following a comprehensive evaluation of several gradient boosting algorithms, including LightGBM, XGBoost, and CatBoost, among which LightGBM showed better performance in the training efficiency and prediction accuracy (Text S1 and Table S2). During the data set preparation for ML, we conduct feature selection, correlation analysis, and filtering (see Text S2 for details). The input features for the ML model include meteorological variables, precursor concentrations, and photolysis rate constants from CESM2 outputs, along with the spatial information on each monitoring site, as summarized in Table S3. These variables have been previously applied to construct regression models of ozone deviations between modeled and observed ozone concentrations.[35] To improve model interpretability, we employ Gini-Importance and SHAP values, both widely used in air quality predictions (see Text S3 for more details).

In this study, the LightGBM method is applied to construct calibration models. Specifically, samples over 2014−2018 are used for model training, while those for 2019 are utilized to validate the ML model performance. During the model training process, 20% of the data are selected to optimize the hyperparameter combination with the aid of the Optuna tool, which is a Python-based automated hyperparameter optimization framework. It is a Bayesian optimization algorithm based on probabilistic models, which can find the optimal solution by continuously exploring and leveraging existing information.[60]

The performance of the model is further evaluated by using R^2, mean absolute error (MAE), and root mean squared error (RMSE) to determine the accuracy and reliability of the predictions. The density scatter plots of the validation set demonstrate the excellent performance of the models for China, the United States, and Europe, with R^2 values higher than 0.8 and MAE values of about 2−3 $\mu g/m^3$ (Figure S3). To quantify the uncertainty associated with the ML correction, we further examined the distribution of the residuals beyond the standard performance metrics (MAE, RMSE, R^2). Across the regions, the mean residuals remain close to zero (−0.02 to 0.01 $\mu g/m^3$), indicating that the correction does not introduce an additional systematic bias (Table S4). To assess the spatial robustness of ML considering model extrapolation, we also employ a site-based spatial retention method with a buffer exclusion mechanism (see Text S4 for details). Using this approach, the model achieved a spatial R^2 of approximately 0.8 (Table S5), indicating strong generalization capability across the sites of this ML-based bias-correction method.

The predicted bias B_{ML} was then subtracted from CESM2 outputs to obtain bias-corrected ozone fields

$$O_{3\ \mathrm{corrected}}(i, t) = O_{3\ \mathrm{CESM2}}(i, t) - B_{\mathrm{ML}}(X_{i,t})$$

where $X_{i,t}$ denotes the vector of predictor variables (e.g., meteorological fields, precursor concentrations, and spatial data) at grid cell i and time t.

Correcting the CESM2 results with the ML model offers a method to improve future projections by quantifying the deviations of the modeled results from observed ozone concentrations and under-

https://doi.org/10.1021/acs.est.5c11992
Environ. Sci. Technol. 2026, 60, 3135−3147

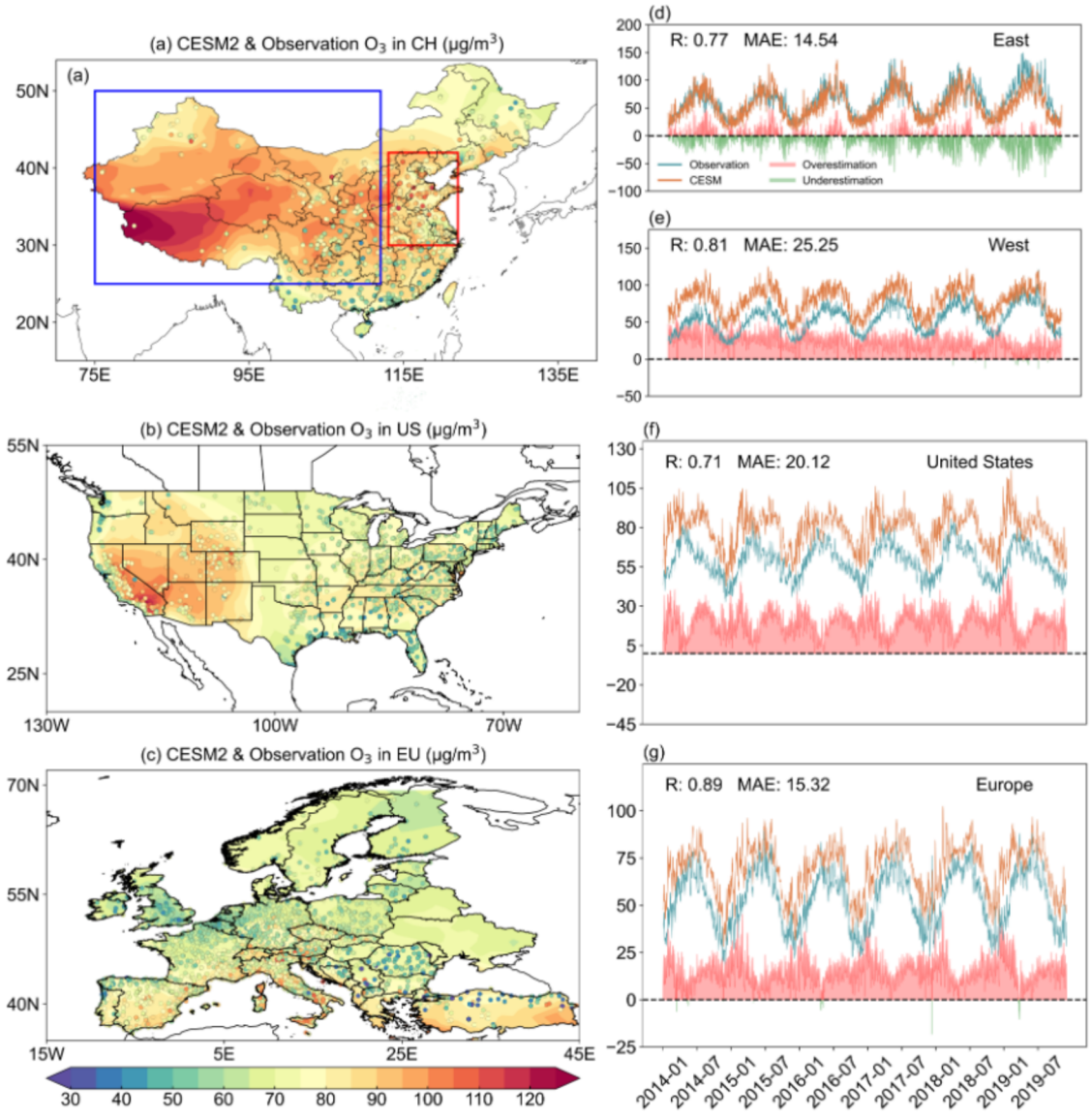

Figure 1. (a−c) Spatial distribution of CESM2-simulated and observed warm season (April−September) mean surface ozone concentrations (μg/m^3) averaged over 2014−2019 in China, the United States, and Europe. (d−g) Time series of CESM2-simulated ozone concentrations, observations, and their differences at observational sites in eastern China (113°−122°E, 30°−42°N), western China (75°−112°E, 25°−50°N), the United States, and Europe ($R = \frac{\sum_{i=1}^{n}(x_i-\bar{x})(y_i-\bar{y})}{\sqrt{\sum_{i=1}^{n}(x_i-\bar{x})^2\sum_{i=1}^{n}(y_i-\bar{y})^2}}$, $\mathrm{MAE} = \frac{1}{n}\sum_{i=1}^{n}|y_i-\hat{y}_i|$).

standing the relationships among various influencing variables. It enables the estimation of potential future biases based on relevant variables in the model simulations.

3. RESULTS

3.1. Ozone Bias in CMIP6 Models and CESM2 Simulations

Earth system models are essential tools for understanding changes across the Earth's various components. However, due to simplifications in model processes and computational constraints, model biases in atmospheric constituents are inevitable, especially those related to complex atmospheric chemistry. Figure 1a,1b presents the multimodel ensemble mean distribution of CMIP6 simulated surface ozone concentration for the warm season (April−September) and their biases relative to observations. The time series of simulated and observed values, along with their biases, for China, Europe, and the United States during 2015−2019 are shown in Figure S4c−e (the distributions of individual model results are provided in Figure S5). The simulations from CMIP6 models indicate that globally high surface ozone concentrations are primarily distributed between 30°N and 60°N. Although models can capture the temporal ozone variation, with correlation coefficients between simulations and observations higher than 0.8, they tend to overestimate ozone concentrations in China, Europe, and the United States. In China, the overall temporal correlation coefficient is 0.81, with a MAE of 20.2 μg/m^3. The simulation results exhibit contrasting biases between eastern and western China (Figure S6). In eastern China (113°−122°E, 30°−42°N), particularly the North China Plain, the model tends to underestimate ozone levels by 17.1 μg/m^3 during the warm season. In contrast, western China (75°−112°E, 25°−50°N) is predominantly characterized by model overestimation, with an MAE of 30.5 μg/m^3. In the United States and Europe, the models

https://doi.org/10.1021/acs.est.5c11992
Environ. Sci. Technol. 2026, 60, 3135−3147

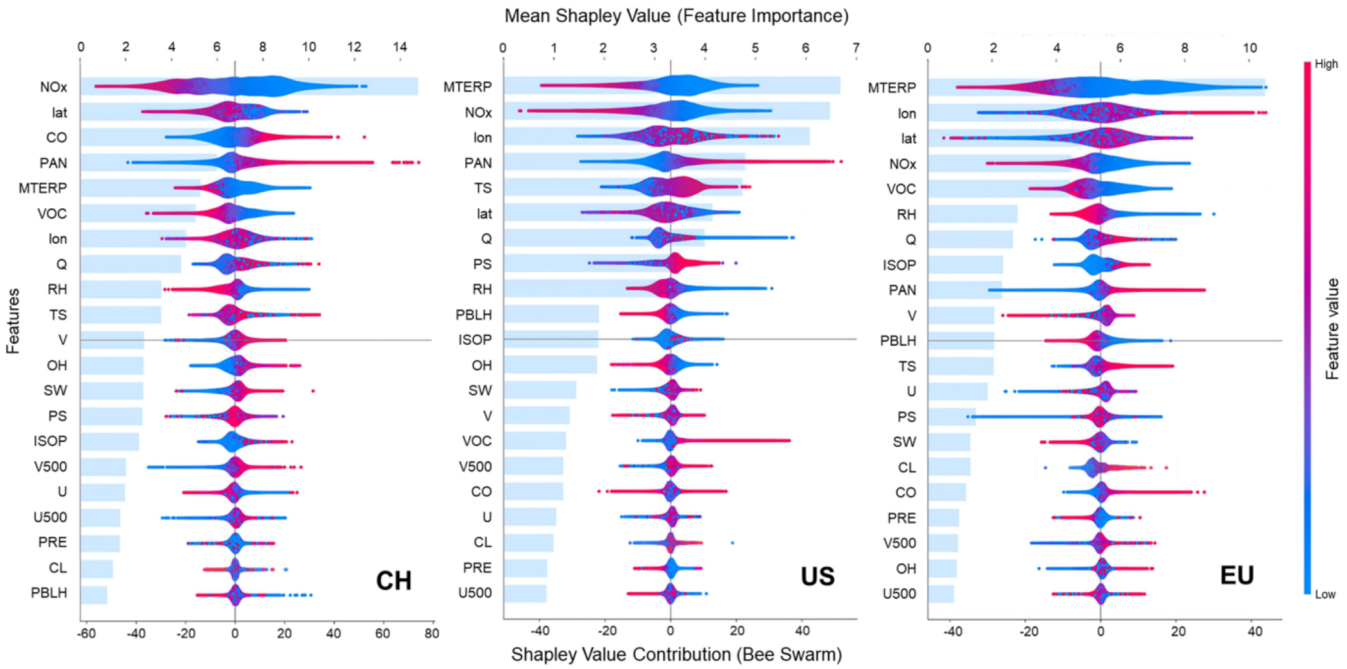

Figure 2. SHAP analysis and relative feature importance across the three regional models for ozone bias in China (CH), the United States (US), and Europe (EU). The blue bars represent the absolute mean SHAP values, reflecting the average contribution of each feature to the model's predictions. The accompanying bee swarm plots display the distribution of SHAP values for each feature, with the color gradient from blue to red indicating low to high feature values.

generally overestimate surface ozone concentrations with MAEs of 24.3 and 28.4 $\mu g/m^3$, respectively (Figure S7).

Given the substantial and non-negligible model biases, it is desirable to correct the model outputs before future projection. Here, we use CESM2, a member of the CMIP6 models, as an example to perform bias correction and to project future ozone concentrations. According to Figure 1, comparison between CESM2-simulated ozone concentrations and observational data also reveals notable deviations. CESM2 underestimates ozone concentrations in eastern China and overestimates them in western China during the warm season over 2014−2019, exhibiting a spatial dipole pattern of ozone biases similar to that in CMIP6 results.

The seasonal bias in surface ozone concentrations in eastern China, where CESM2 underestimates ozone concentrations during the cold season and overestimates them during the warm season, primarily stems from the MOZART-T1 chemical mechanism, the characterization of oxidant and deposition processes, and coarse model resolution.[61] During the cold season, lower OH concentrations and reduced nitrate cycling suppress ozone production, leading to the underestimation. Conversely, during the warm season, enhanced photochemical processes and insufficient characterization of ozone precursors result in excessive ozone production, leading to the ozone overestimation.[47] The biases in western China are likely attributed to the relatively low anthropogenic precursor emissions, different boundary layer dynamics, and bias in regional transport in this region. Ozone concentrations in southern China are also overestimated by the model, likely attributed to the relatively low anthropogenic precursor emissions, consistent with the general tendency of models to underestimate ozone concentrations in high-emission areas and overestimate them in low-emission areas. Beyond emission factors, meteorological factors such as frequent precipitation, high humidity, and oceanic influences in southern China[62,63] also affect ozone formation and transport, potentially leading to model biases. In Europe and the United States, CESM2 consistently overestimates surface ozone concentrations, consistent with CMIP6 results, which is likely due to the similar factors mentioned above.

3.2. Bias Correction by Machine Learning Method

Discrepancies in historical simulations between models and observations indicate potential biases that could also affect future ozone projections. By applying ML techniques to estimate the model biases in historical CESM2 simulations, we can construct an ML model that predicts potential biases in future simulations and removes them by subtracting the ML-predicted values from the CESM2 future projection. Based on prior knowledge and key ozone-influencing factors, we initially select 26 features, remove highly correlated ones (Figure S8), and train LightGBM models using the remaining 21 features, including meteorological variables, precursor gas concentrations, and spatial information. Separate LightGBM models have been developed for predicting ozone biases in China, the United States, and Europe. The SHAP analysis (Figure 2) and Gini Importance (Figure S9) are employed to enhance interpretability.

In the analysis of the simulated ozone bias in China, the concentration of NO_x is identified as the most important feature. It indicates that NO_x plays a critical role in predicting model biases in China, due to its significant and nonlinear influence on atmospheric chemical processes. Additionally, the model's limited ability to accurately simulate NO_x concentrations (Figure S10) also contributes to the observed deviations. Monoterpenes (MTERP), one of the major volatile organic compounds (VOCs), as well as NO_x, also emerge as a key feature in the ML models for Europe and the United States, indicating their significant influences on bias prediction. Across all three regional models, low biases of ozone tend to

https://doi.org/10.1021/acs.est.5c11992
Environ. Sci. Technol. 2026, 60, 3135−3147

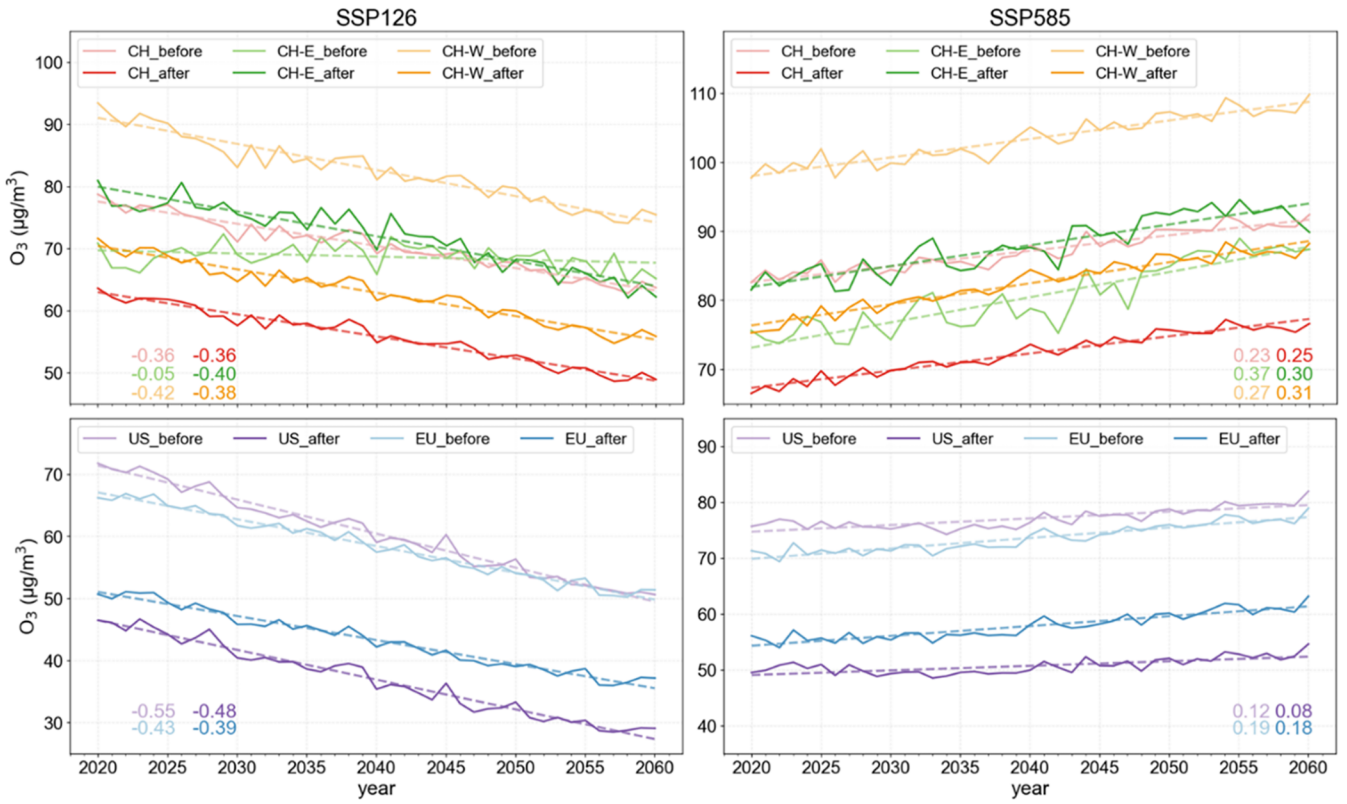

Figure 3. Time series of warm-season mean surface ozone concentrations ($\mu g/m^3$) from 2020 to 2060 over China (CH, top), the United States, and Europe (US and EU, bottom) under SSP1−2.6 (left) and SSP5−8.5 (right) before and after the ML-based bias correction, with the linear trends shown at the bottom of each panel.

occur when NO_x and MTERP concentrations are high, whereas high PAN levels are associated with ozone overestimation. In addition to precursor concentrations, meteorological parameters, especially temperature and humidity, are key factors affecting model biases. The Gini-Importance analysis results are largely consistent with the key features identified by SHAP.

In the original CESM2 results, the model simulations failed to accurately capture the spatial distribution of ozone concentrations in China and tended to overestimate levels in Europe and the United States. With the help of bias correction using ML models trained with data from 2014 to 2018, the CESM2-simulated ozone bias in 2019 can be significantly reduced over the three focused regions (Figure S11). In China, the spatial correlation coefficient between the observed and simulated ozone concentration during the warm season can be increased from 0.2 to 0.8 by incorporating ML-based bias correction, which reduced the bias by approximately 61.2% in terms of MAE. For the United States and Europe, the correlation coefficients increase from 0.7 to 0.9 and from 0.4 to 0.7, respectively. Meanwhile, the biases are reduced by 48.1 and 41.3% in these two regions. These results demonstrate that the ML correction successfully improves the spatial agreement between modeled and observed ozone concentrations and also reproduces historical ozone trends, such as the significant increase in China's warm-season ozone concentrations, while trends in the United States and Europe remain relatively stable.[64] Building upon this ML-based bias correction, we further investigate the future ozone variations in the next section.

3.3. Future Projection in Ozone Driven by Changing Climate and Emissions

Applying the ML-based bias correction to CESM2 ozone predictions, the warm-season mean ozone concentrations show continuous decreases in China, the United States, and Europe during 2020−2060 under the low-emission scenario SSP1−2.6 with trends of −3.6 to −4.8 $\mu g/m^3$/decade, while they are predicted to increase at rates of 0.8−2.5 $\mu g/m^3$/decade under the extreme warming scenario SSP5−8.5 (Figure 3). Considering both the changing climate and anthropogenic emissions, future ozone concentrations are projected to decrease across China, the United States, and Europe, with regional averages of −13.5, −17.9, and −13.7 $\mu g/m^3$ between 2020 and 2060 under SSP 1−2.6. On the contrary, ozone concentrations are projected to increase by 9.4, 2.0, and 5.2 $\mu g/m^3$ over China, the United States, and Europe, respectively, between 2020 and 2060 under SSP 5−8.5.

By decomposing the ozone change to the influences of emissions and climate change, it shows that emissions exert primary roles in the future changes in ozone concentrations in the three key regions under both the SSP1−2.6 and SSP5−8.5 scenarios. In the SSP1−2.6 scenario, emission reductions lead to substantial decreases in ozone levels by 13.1 $\mu g/m^3$ in China, 18.3 $\mu g/m^3$ in the United States, and 14.6 $\mu g/m^3$ in Europe between 2020 and 2060. However, in the SSP5−8.5 scenario, ozone concentrations increase, albeit to a lesser extent, by 8.6 $\mu g/m^3$ in China, 4.6 $\mu g/m^3$ in the United States, and 6.1 $\mu g/m^3$ in Europe.

The impacts of climate change on future ozone variations are also significant, especially under an extreme warming scenario. Unlike the relatively uniform impact of emissions, the

https://doi.org/10.1021/acs.est.5c11992
Environ. Sci. Technol. 2026, 60, 3135−3147

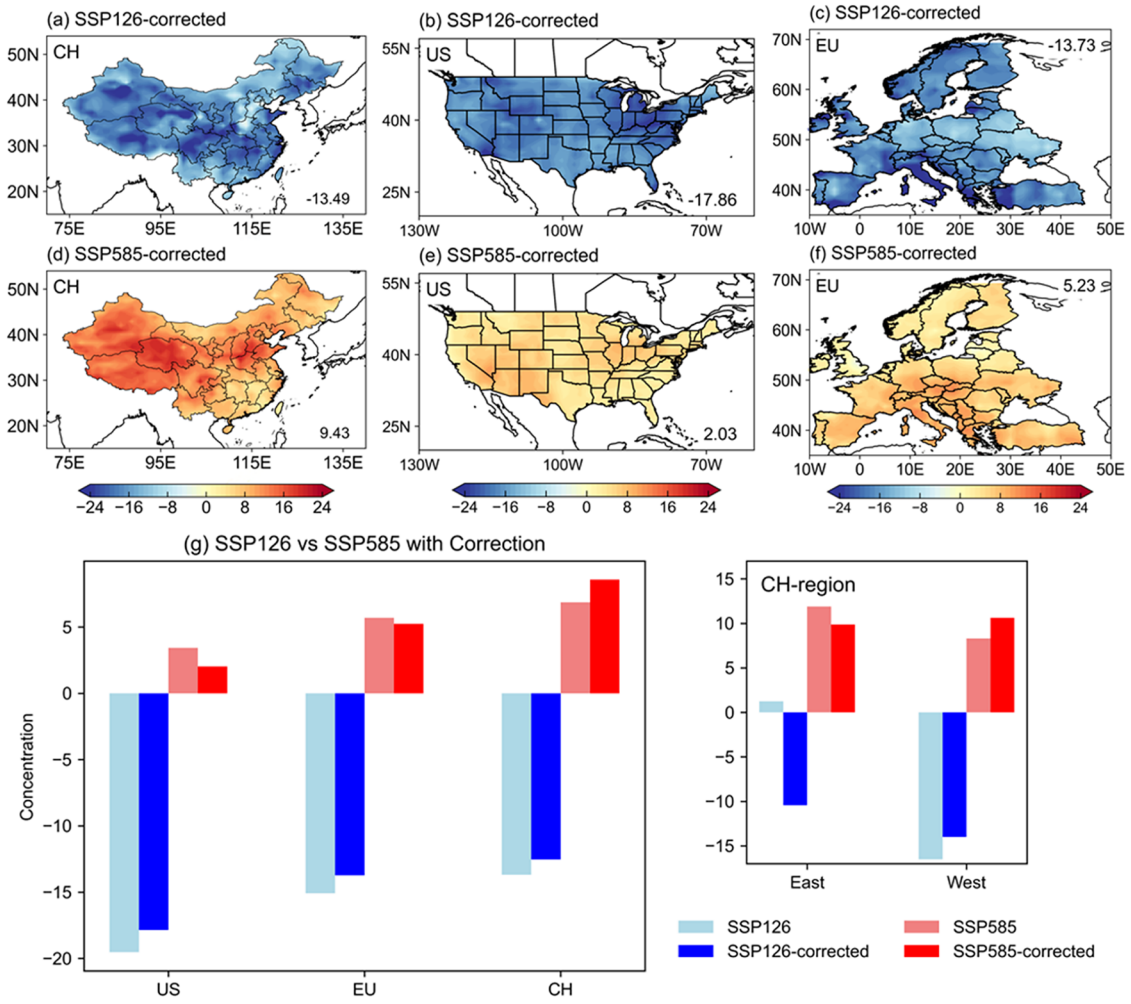

Figure 4. Spatial distribution of CESM2-simulated future changes in warm-season mean surface ozone concentrations ($\mu g/m^3$) in 2060 relative to 2020 over (a, d) China (CH), (b, e) the United States (US), and (c, f) Europe (EU) under SSP1−2.6 (top) and SSP5−8.5 (bottom) scenarios after the bias correction based on ML. (g) Regional averaged changes of warm-season mean surface ozone concentrations ($\mu g/m^3$) over the United States, Europe, and China, as well as eastern China (East) and western China (West), in 2060 relative to 2020 under SSP1−2.6 and SSP5−8.5 scenarios before and after ML-based bias correction.

influence of climate change on ozone concentrations exhibits notable spatial variability across all three regions. Under the SSP1−2.6 scenario, climate change drives an overall increase of 0.6 $\mu g/m^3$ in ozone concentrations across China, with the eastern region experiencing a more pronounced rise of approximately 3.0 $\mu g/m^3$, while the western region experiences a decrease. In the United States and Europe, climate impacts are more spatially heterogeneous, characterized by minor increases and decreases, resulting in overall increases of 0.5 and 0.9 $\mu g/m^3$, respectively. Under the SSP5−8.5 scenario, China exhibits an east-to-west gradient, where ozone concentrations increase by a regional average of 3.1 $\mu g/m^3$ in the east but decrease by 0.5 $\mu g/m^3$ in the west, offsetting each other and leading to a negligible net change of 0.03 $\mu g/m^3$ over China. Meanwhile, the United States and Europe show predominantly decreasing trends under SSP5−8.5, with overall ozone reductions by 2.6 and 0.9 $\mu g/m^3$, respectively. The influences of climate change on ozone concentrations in China in this study are similar to the findings in Li et al.[65,66] based on ML prediction and in Zhu et al.[13] based on single model simulations that climate change would enhance ozone pollution in polluted eastern China and mitigate it in western China.

The spatial variability in climate-induced ozone changes is due to nonlinear interactions between meteorological factors, such as temperature and humidity, and ozone chemistry (Figure S12). For example, in the polluted eastern China, higher temperatures enhance photochemical reactions, accelerating ozone formation in NO_x-rich environments under SSP5−8.5, which reveals a strong climate penalty on ozone pollution over this region.[67] Although temperatures do not present considerable changes under SSP1−2.6, the decrease in humidity remains favorable for ozone production. In contrast, western China experiences increased humidity, which suppresses ozone formation through enhanced radical termination reactions and reduced photolysis rates. In the United States and Europe, the increases in humidity under SSP5−8.5 also lead to decreases in ozone concentrations over these regions. These demonstrate the climate penalty and benefits from ozone pollution that should be considered in future ozone projections.

https://doi.org/10.1021/acs.est.5c11992
Environ. Sci. Technol. 2026, 60, 3135−3147

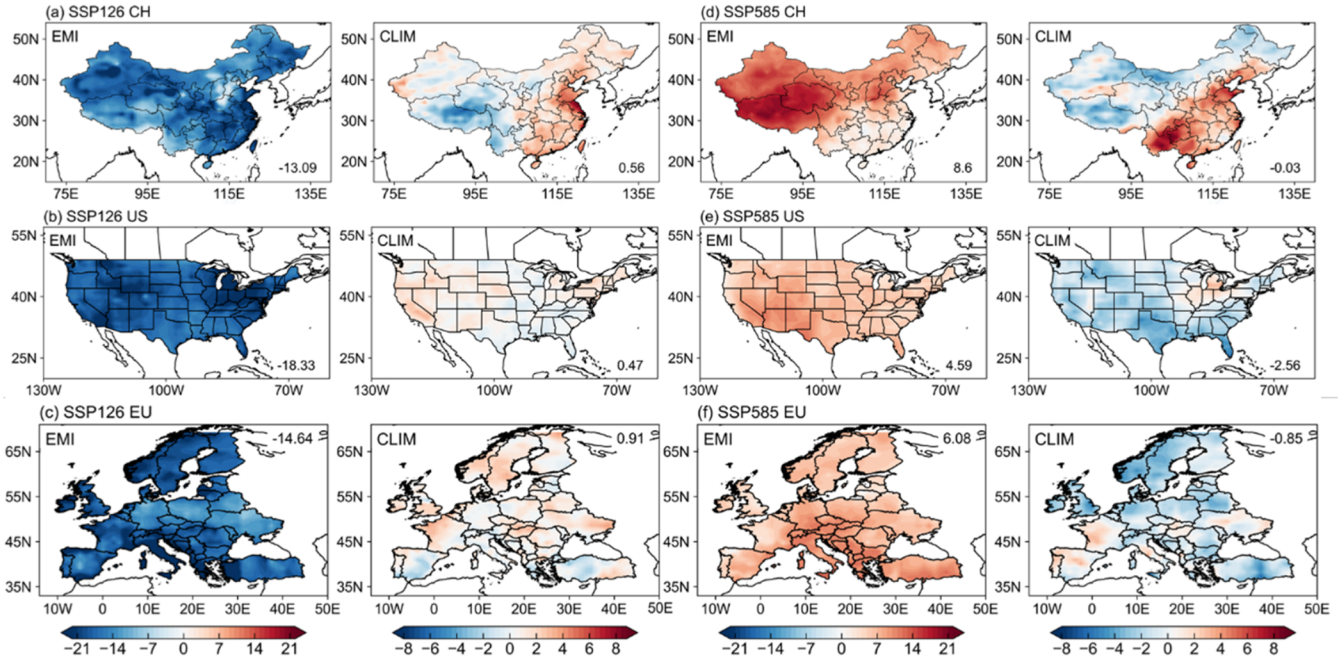

Figure 5. Effects of future changes in anthropogenic emissions (EMI) and climate (CLIM) on the differences in warm-season mean surface ozone concentrations ($\mu g/m^3$) over (a, d) China, (b, e) the United States, and (c, f) Europe between 2020 and 2060 under the SSP1−2.6 and SSP5−8.5 after bias correction. Regional average is shown in the right corner of each panel.

3.4. Effect of ML-Based Bias Correction on Future Ozone Prediction

As shown by comparing the future variations of ozone concentrations before and after bias correction (Figure 3), the ML method effectively reduces overall ozone concentrations over western China, the United States, and Europe, but does not largely affect their trends. Over eastern China, ML can also enhance ozone concentrations under the SSP5−8.5 scenario but retain its increasing trends. However, the ML-based bias correction converts the insignificant trend of −0.5 $\mu g/m^3$/decade over eastern China under SSP1−2.6 to the strong decreasing trend by −4.0 $\mu g/m^3$/decade. Relative to 2020, CESM2 predicts a slight increase in ozone concentration in eastern China by 1.3 $\mu g/m^3$ in 2060 under SSP1−2.6 (Figures 4 and S13). With the ML bias correction, it reverses to a sharp decrease of 10.4 $\mu g/m^3$. Based on the GCAP2 model framework, Kang et al.[68] examined future changes in ozone levels in China under a carbon neutrality scenario SSP1−1.9, similar to SSP1−2.6 used in this study. They found that emission changes would significantly decrease ozone concentrations in eastern China during 2010−2045, while climate change would slightly increase them in the same period. It supports the finding that the original CESM2 may underestimate the ozone decrease over polluted eastern China under the low-emission scenario. These results also indicate that the ML-based bias correction can not only improve model representation of the surface ozone concentrations in both spatial distribution and magnitude but also correct the long-term variation of regional ozone.

The potential error of the predicted ozone trend in eastern China under the SSP1−2.6 scenario can be attributed to both emission- and climate-driven photochemical processes. In the original model output, anthropogenic emissions lead to increased ozone concentrations in eastern China, even though the precursor NO_x and VOCs are substantially reduced, and the ozone increase is further amplified by the impact of SST/SIC-related climate change (Figure S14). After ML-based bias correction, emission reductions no longer elevate ozone in the east but instead contribute to a decline, while the climate-driven ozone increase also becomes less pronounced (Figure 5). First of all, the reversal of ozone trends in eastern China can be interpreted as an adaptive adjustment by the model to its previous misjudgment of the nonlinear relationship between precursors and ozone concentrations. SHAP analysis indicates that NO_x is a critical factor in predicting model bias, particularly in China, where low NO_x concentrations tend to lead to model overestimation of ozone. As the substantial reductions in NO_x emissions in the polluted eastern China under the low-emission scenario, the negative bias shifts to a positive bias (Figure 3), leading to the incorrectly predicted insignificant or even increasing trend of ozone in eastern China. In addition, the climate-driven ozone increases are weakened after bias correction, which may be partly related to the photochemical process associated with meteorological conditions. SHAP analysis indicates that variables, such as temperature and humidity, significantly contribute to model bias. Sensitivity to temperature and inadequate characterization of humidity-related radical termination and photolysis inhibition may lead to biases in ozone production.

4. DISCUSSION

This study demonstrates that many CMIP6 models, including CESM2, exhibit systematic biases in simulating surface ozone concentrations over major regions, such as China, the United States, and Europe. To address this issue, we applied an ML approach to correct biases in CESM2 model outputs based on the meteorological variables, precursor gas concentrations, and spatial information. The ML bias correction significantly improved the spatial distributions and reduced the biases across all three regions. Applying ML-based bias correction to CESM2 future projections driven by both changes in anthropogenic emissions and climate change reveals distinct

https://doi.org/10.1021/acs.est.5c11992
Environ. Sci. Technol. 2026, 60, 3135−3147

regional ozone trends under different emission scenarios during 2020−2060.

A cross-regional comparison among China, the United States, and Europe reveals distinct patterns for future ozone responses. Under SSP1−2.6, all three regions experience declining ozone driven largely by reductions in anthropogenic precursor emissions, with stronger decreases in the United States and Europe, where emission controls are more advanced.[2] Under SSP5−8.5, ozone increases are largest in China, moderate in Europe, and weakest in the United States, reflecting regional disparities in precursor emission growth and the magnitude of climate-driven ozone penalties.

Our results are consistent with previous CMIP6-based studies that show emission changes dominate future ozone trends, while climate change also exerts important roles in regulating ozone concentrations. For example, studies have concluded that ozone concentrations tend to decrease under low-emission scenarios and increase under high-emission scenarios.[69] Zanis et al.[67] analyzed the impact of climate change on global surface ozone using CMIP6 model results and found that climate change generally reduces ozone levels in regions far away from pollution sources but may worsen ozone pollution near emission hotspots. This study advances prior work by applying ML-based bias correction to the model outputs, enabling finer-scale attribution of regional ozone changes and improving the future prediction of ozone pollution.

There are some limitations in this study. Model bias mainly stems from systematic limitations in chemical mechanisms, deposition processes, spatial resolution, and representation of precursor emissions. ML-based bias correction in this study can reduce such systematic bias by learning the relationships between modeled ozone biases and other related variables, without directly correcting the physical and chemical processes. It should be caution that although the predictor distributions of meteorological variables remain largely consistent between historical and future periods, substantial changes in emission-related variables (e.g., NO_x and VOCs) may introduce additional uncertainties into the model predictions, particularly under SSP1−2.6, where significant emission reductions are projected relative to the present-day level. Also, this study conducted a detailed analysis for China, the United States, and Europe, but ozone projections and bias corrections in other areas are also noteworthy. Fang et al.[70] found that ozone pollution in Southeast Asia was also severe, and synergistic control of NO_x and VOCs under low-emission strategies would be needed in the future to reduce ozone-related premature deaths. With sufficient observational data, this ML-based method could also be applied to other regions, such as Southeast Asia, India, and Africa, where ozone pollution poses growing concerns. Expanding the regional coverage will be a valuable step in future work, particularly as more monitoring data becomes available. Although we have analyzed three key regions and refined the differences between eastern and western China, the inherent limitations of model resolution and the uneven distribution of ground observation stations remain major sources of uncertainty.[71] Since machine learning models rely on observable spatial gradients and regional-scale meteorological-chemical backgrounds, the spatial structure of ozone in sparsely observed regions often cannot be fully learned, leading to relatively high prediction errors. Therefore, integrating higher-resolution model simulations with more comprehensive observation systems will be a key direction for reducing spatial uncertainty and enhancing the reliability of regional- and even global-scale predictions in the future.

This study simplifies the characterization of climate change, mainly through changes in SST and SIC in model simulations. Because the ocean stores over 90% of the global energy imbalance, SST anomalies strongly regulate large-scale temperature, humidity, and circulation fields, which in turn shape ozone production and transport.[72] Thus, many climate-related forcings, such as greenhouse gas increases, aerosols, and remote land-surface changes, are implicitly reflected in the SST/SIC-driven responses. Since oceanic changes are the primary focus, this framework has certain weaknesses, as it may not fully capture variations in land-surface temperatures. Future research is expected to utilize fully coupled Earth system models to quantify the effects of other external forcings, such as changes in aerosols, land use, and biogenic emissions.

Although this study uses CESM2 as a demonstration model, the proposed ML correction method is applicable to other CMIP6 models, offering a generalizable approach for reducing model biases in simulating ozone concentrations. While interpretable ML techniques help identify the drivers of model bias, some biases between the simulated and observed values remain unexplained. Also, this ML framework primarily addresses existing biases between model and observation, while uncertainties associated with the model's ability to predict future ozone may still constitute a potential source of biases. The interpretable ML techniques we applied offer explanations through mathematical and statistical means, but cannot fully substitute for the physicochemical mechanisms explicitly represented by the atmospheric model equations. Instead, they provide complementary diagnostic insights, including the identification of key chemical and meteorological drivers of bias, which may guide future model development and parameter tuning. In particular, the interpretability methods used in this study (SHAP values and Gini importance) help reveal how individual predictors influence the model errors, thereby offering physically meaningful clues for refining chemical mechanisms and improving process representations in CESM2.

Overall, this study highlights the potential of combining Earth system model simulations and ML-based bias correction to produce more accurate projections of ozone pollution, thereby supporting more effective and region-specific air quality policies. Future ML models that incorporate a broader range of process variables may further elucidate the root causes of model errors. This insight can guide modifications to model input parameters and refinements of the relevant physicochemical processes and numerical equations to address the inferred sources of bias.

■ ASSOCIATED CONTENT

Data Availability Statement

Surface ozone observations over China can be obtained from the China National Environmental Monitoring Center (http://www.cnemc.cn). In Europe, surface ozone data encompassing 36 countries are available from the European Environment Agency https://discomap.eea.europa.eu/map/fme/AirQualityExport.html. In the United States, surface ozone measurements are sourced from the United States Environmental Protection Agency (https://aqs.epa.gov/aqsweb/airdata/download_files.html#Daily;EPA, 2023).

https://doi.org/10.1021/acs.est.5c11992
Environ. Sci. Technol. 2026, 60, 3135−3147

Supporting Information

The Supporting Information is available free of charge at https://pubs.acs.org/doi/10.1021/acs.est.5c11992.

Additional methodological details on machine learning algorithm selection, feature selection, model interpretability, and spatial validation (Texts S1−S4); supporting figures showing emissions, climate drivers, model evaluation, bias correction performance, and future ozone changes (Figures S1−S14); supporting tables summarizing CMIP6 models, machine learning performance metrics, input features, uncertainty statistics, and spatial validation results (Tables S1−S5) (PDF)

AUTHOR INFORMATION

Corresponding Author

Yang Yang − *State Key Laboratory of Climate System Prediction and Risk Management/Jiangsu Key Laboratory of Atmospheric Environment Monitoring and Pollution Control/Jiangsu Collaborative Innovation Center of Atmospheric Environment and Equipment Technology/Joint International Research Laboratory of Climate and Environment Change, Nanjing University of Information Science and Technology, Nanjing, Jiangsu 210044, China; School of Environmental Science and Engineering, Nanjing University of Information Science and Technology, Nanjing, Jiangsu 210044, China;* orcid.org/0000-0002-9008-5137; Email: yang.yang@nuist.edu.cn

Authors

Yiqian Ni − *State Key Laboratory of Climate System Prediction and Risk Management/Jiangsu Key Laboratory of Atmospheric Environment Monitoring and Pollution Control/Jiangsu Collaborative Innovation Center of Atmospheric Environment and Equipment Technology/Joint International Research Laboratory of Climate and Environment Change, Nanjing University of Information Science and Technology, Nanjing, Jiangsu 210044, China; School of Environmental Science and Engineering, Nanjing University of Information Science and Technology, Nanjing, Jiangsu 210044, China;* orcid.org/0009-0007-8773-3854

Hailong Wang − *Atmospheric, Climate, and Earth Sciences Division, Pacific Northwest National Laboratory, Richland, Washington 99352, United States;* orcid.org/0000-0002-1994-4402

Pinya Wang − *School of Environmental Science and Engineering, Nanjing University of Information Science and Technology, Nanjing, Jiangsu 210044, China*

Ke Li − *State Key Laboratory of Climate System Prediction and Risk Management/Jiangsu Key Laboratory of Atmospheric Environment Monitoring and Pollution Control/Jiangsu Collaborative Innovation Center of Atmospheric Environment and Equipment Technology/Joint International Research Laboratory of Climate and Environment Change, Nanjing University of Information Science and Technology, Nanjing, Jiangsu 210044, China; School of Environmental Science and Engineering, Nanjing University of Information Science and Technology, Nanjing, Jiangsu 210044, China;* orcid.org/0000-0002-9181-3562

Lei Chen − *School of Environmental Science and Engineering, Nanjing University of Information Science and Technology, Nanjing, Jiangsu 210044, China;* orcid.org/0000-0003-1409-8371

Jia Zhu − *School of Environmental Science and Engineering, Nanjing University of Information Science and Technology, Nanjing, Jiangsu 210044, China*

Baojie Li − *School of Environmental Science and Engineering, Nanjing University of Information Science and Technology, Nanjing, Jiangsu 210044, China;* orcid.org/0000-0002-3747-6534

Hong Liao − *State Key Laboratory of Climate System Prediction and Risk Management/Jiangsu Key Laboratory of Atmospheric Environment Monitoring and Pollution Control/Jiangsu Collaborative Innovation Center of Atmospheric Environment and Equipment Technology/Joint International Research Laboratory of Climate and Environment Change, Nanjing University of Information Science and Technology, Nanjing, Jiangsu 210044, China; School of Environmental Science and Engineering, Nanjing University of Information Science and Technology, Nanjing, Jiangsu 210044, China;* orcid.org/0000-0001-6628-1798

Complete contact information is available at: https://pubs.acs.org/10.1021/acs.est.5c11992

Notes

The authors declare no competing financial interest.

ACKNOWLEDGMENTS

This study was supported by the National Natural Science Foundation of China (grants 42293320 and 42475032) and the Jiangsu Innovation and Entrepreneurship Team (grant JSSCTD202346). Pacific Northwest National Laboratory is operated for DOE by the Battelle Memorial Institute under contract DE-AC05-76RL01830.

REFERENCES

(1) Gaudel, A.; Cooper, O. R.; Ancellet, G.; Barret, B.; Boynard, A.; Burrows, J. P.; Clerbaux, C.; Coheur, P.-F.; Cuesta, J.; Cuevas, E.; Doniki, S.; Dufour, G.; Ebojie, F.; Foret, G.; Garcia, O.; Granados-Muñoz, M. J.; Hannigan, J. W.; Hase, F.; Hassler, B.; Huang, G.; Hurtmans, D.; Jaffe, D.; Jones, N.; Kalabokas, P.; Kerridge, B.; Kulawik, S.; Latter, B.; Leblanc, T.; Le Flochmoën, E.; Lin, W.; Liu, J.; Liu, X.; Mahieu, E.; McClure-Begley, A.; Neu, J. L.; Osman, M.; Palm, M.; Petetin, H.; Petropavlovskikh, I.; Querel, R.; Rahpoe, N.; Rozanov, A.; Schultz, M. G.; Schwab, J.; Siddans, R.; Smale, D.; Steinbacher, M.; Tanimoto, H.; Tarasick, D. W.; Thouret, V.; Thompson, A. M.; Trickl, T.; Weatherhead, E.; Wespes, C.; Worden, H. M.; Vigouroux, C.; Xu, X.; Zeng, G.; Ziemke, J. Tropospheric Ozone Assessment Report: Present-day distribution and trends of tropospheric ozone relevant to climate and global atmospheric chemistry model evaluation. *Elem. Sci. Anth.* **2018**, *6*, No. 39.

(2) Young, P. J.; Naik, V.; Fiore, A. M.; Gaudel, A.; Guo, J.; Lin, M. Y.; Neu, J. L.; Parrish, D. D.; Rieder, H. E.; Schnell, J. L.; Tilmes, S.; Wild, O.; Zhang, L.; Ziemke, J.; Brandt, J.; Delcloo, A.; Doherty, R. M.; Geels, C.; Hegglin, M. I.; Hu, L.; Im, U.; Kumar, R.; Luhar, A.; Murray, L.; Plummer, D.; Rodriguez, J.; Saiz-Lopez, A.; Schultz, M. G.; Woodhouse, M. T.; Zeng, G. Tropospheric Ozone Assessment Report: Assessment of global-scale model performance for global and regional ozone distributions, variability, and trends. *Elem. Sci. Anth.* **2018**, *6*, No. 10.

(3) Gonzalez-Abraham, R.; Chung, S. H.; Avise, J.; Lamb, B.; Salathé, E. P.; Nolte, C. G.; Streets, D. G.; et al. The effects of global change upon United States air quality. *Atmos. Chem. Phys.* **2015**, *15*, 12645−12665.

(4) Goldberg, D. L.; Anenberg, S. C.; Lu, Z.; Streets, D. G.; Lamsal, L. N.; McDuffie, E. E.; Smith, S. J. Urban NOX emissions around the world declined faster than anticipated between 2005 and 2019. *Environ. Res. Lett.* **2021**, *16*, No. 115004.
(5) Shaw, S.; Van Heyst, B. Nitrogen Oxide (NOX) emissions as an indicator for sustainability. *Environ. Sustain. Indic.* **2022**, *15*, No. 100188.
(6) Crippa, M.; Guizzardi, D.; Butler, T.; Keating, T.; Wu, R.; Kaminski, J.; Kuenen, J.; Kurokawa, J.; Chatani, S.; Morikawa, T.; Pouliot, G.; Racine, J.; Moran, M. D.; Klimont, Z.; Manseau, P. M.; Mashayekhi, R.; Henderson, B. H.; Smith, S. J.; Suchyta, H.; Muntean, M.; Solazzo, E.; Banja, M.; Schaaf, E.; Pagani, F.; Woo, J.-H.; Kim, J.; Monforti-Ferrario, F.; Pisoni, E.; Zhang, J.; Niemi, D.; Sassi, M.; Ansari, T.; Foley, K. The HTAP_v3 emission mosaic: merging regional and global monthly emissions (2000−2018) to support air quality modelling and policies. *Earth Syst. Sci. Data* **2023**, *15*, 2667−2694.
(7) Cooper, O. R.; Parrish, D. D.; Ziemke, J.; Balashov, N. V.; Cupeiro, M.; Galbally, I. E.; Gilge, S.; Horowitz, L.; Jensen, N. R.; Lamarque, J.-F.; Naik, V.; Oltmans, S. J.; Schwab, J.; Shindell, D. T.; Thompson, A. M.; Thouret, V.; Wang, Y.; Zbinden, R. M. Global distribution and trends of tropospheric ozone: An observation-based review. *Elem. Sci. Anth.* **2014**, *2* (1), No. 000029.
(8) Chang, K.-L.; Petropavlovskikh, I.; Cooper, O. R.; Schultz, M. G.; Wang, T. Regional trend analysis of surface ozone observations from monitoring networks in eastern North America, Europe and East Asia. *Elem. Sci. Anth.* **2017**, *5* (1), No. 50.
(9) Fleming, Z. L.; Doherty, R. M.; von Schneidemesser, E.; Malley, C. S.; Cooper, O. R.; Pinto, J. P.; Colette, A.; Xu, X.; Simpson, D.; Schultz, M. G.; Lefohn, A. S.; Hamad, S.; Moolla, R.; Solberg, S.; Feng, Z. Tropospheric Ozone Assessment Report: Present-day ozone distribution and trends relevant to human health. *Elem. Sci. Anth.* **2018**, *6* (1), No. 12.
(10) Mills, G.; Pleijel, H.; Malley, C. S.; Sinha, B.; Cooper, O. R.; Schultz, M. G.; Neufeld, S.; Gerosa, A.; Tarasick, A. W.; Law, R. M.; Dentener, F. J.; Stevenson, R. E.; Monks, P. S.; Schultz, J. F.; Turnock, S. T.; Smith, S. J.; Granier, V.; Hicks, C.; Young, P. J.; Wild, P. J.; Steiner, S. T.; Conley, A. J.; van Marle, C. J. A. M.; van Noije, M.; van Noije, T. P. C.; van Velthoven, P. T.; van Velthoven, P. F. J.; Krol, M. C.; Hazeleger, W.; Williams, A. G.; Chambers, S. D.; Le Sager, P.; van Noije, T. Tropospheric Ozone Assessment Report: Present-day tropospheric ozone distribution and trends relevant to vegetation. *Elem. Sci. Anth.* **2018**, *6* (1), No. 47.
(11) Li, P.; Yang, Y.; Wang, H.; Li, S.; Li, K.; Wang, P.; Li, B.; Liao, H. Source attribution of near-surface ozone trends in the United States during 1995−2019. *Atmos. Chem. Phys.* **2023**, *23*, 5403−5417.
(12) Yang, Y.; Zhou, Y.; Wang, H.; Li, M.; Li, H.; Wang, P.; Yue, X.; Li, K.; Zhu, J.; Liao, H. Meteorological characteristics of extreme ozone pollution events in China and their future predictions. *Atmos. Chem. Phys.* **2024**, *24*, 1177−1191.
(13) Zhu, J.; Yang, Y.; Wang, H.; Gao, J.; Liu, C.; Wang, P.; Liao, H. Impacts of projected changes in sea surface temperature on ozone pollution in China toward carbon neutrality. *Sci. Total Environ.* **2024**, *915*, No. 170024.
(14) Li, K.; Jacob, D. J.; Liao, H.; Shen, L.; Zhang, Q.; Bates, K. H. Anthropogenic drivers of 2013−2017 trends in summer surface ozone in China. *Proc. Natl. Acad. Sci. U.S.A.* **2019**, *116* (2), 422−427.
(15) Kong, L.; Song, M.; Li, X.; Liu, Y.; Lu, S.; Zeng, L.; Zhang, Y. Analysis of China's PM2.5 and ozone coordinated control strategy based on the observation data from 2015 to 2020. *J. Environ. Sci.* **2024**, *138*, 385−394.
(16) Lu, X.; Hong, J.; Zhang, L.; Cooper, O. R.; Schultz, M. G.; Xu, X.; Wang, T.; Gao, M.; Zhao, Y.; Zhang, Y. Severe surface ozone pollution in China: a global perspective. *Environ. Sci. Technol. Lett.* **2018**, *5*, 487−494.
(17) Ni, Y.; Yang, Y.; Wang, H.; Li, H.; Li, M.; Wang, P.; Li, K.; Liao, H. Contrasting changes in ozone during 2019−2021 between eastern and the other regions of China attributed to anthropogenic emissions and meteorological conditions. *Sci. Total Environ.* **2024**, *908*, No. 168272.
(18) Yang, Y.; Li, M.; Wang, H.; Li, H.; Wang, P.; Li, K.; Gao, M.; Liao, H. ENSO modulation of summertime tropospheric ozone over China. *Environ. Res. Lett.* **2022**, *17*, No. 034020.
(19) Li, M.; Yang, Y.; Wang, H.; Wang, P.; Liao, H. Unique impacts of strong and westward-extended western Pacific subtropical high on ozone pollution over eastern China. *Environ. Pollut.* **2024**, *358*, No. 124515.
(20) Qi, C.; Wang, P.; Yang, Y.; Li, H.; Zhang, H.; Ren, L.; Jin, X.; Zhan, C.; Tang, J.; Liao, H. Impacts of tropical cyclone−heat wave compound events on surface ozone in eastern China: comparison between the Yangtze River and Pearl River deltas. *Atmos. Chem. Phys.* **2024**, *24*, 11775−11789.
(21) Liu, S.; Xing, J.; Zhang, H.; Ding, D.; Zhang, F.; Zhao, B.; Sahu, S. K.; Wang, S. Climate-driven trends of biogenic volatile organic compound emissions and their impacts on summertime ozone and secondary organic aerosol in China in the 2050s. *Atmos. Environ.* **2019**, *218*, No. 117020.
(22) Sahu, S. K.; Chen, L.; Liu, S.; Xing, J.; Mathur, R. Effect of Future Climate Change on Stratosphere-to-Troposphere-Exchange Driven Ozone in the Northern Hemisphere. *Aerosol Air Qual. Res.* **2023**, *23*, No. 220414.
(23) Hong, C.; Zhang, Q.; Zhang, Y.; Davis, S. J.; Tong, D.; Zheng, Y.; Liu, Z.; Guan, D.; He, K.; Schellnhuber, H. J. Impacts of climate change on future air quality and human health in China. *Proc. Natl. Acad. Sci. U.S.A.* **2019**, *116*, 17193−17200.
(24) Dewan, S.; Lakhani, A. Tropospheric ozone and its natural precursors impacted by climatic changes in emission and dynamics. *Front. Environ. Sci.* **2022**, *10*, No. 1007942.
(25) Wang, P.; Yang, Y.; Li, H.; Chen, L.; Dang, R.; Xue, D.; Li, B.; Tang, J.; Leung, L. R.; Liao, H. North China Plain as a hot spot of ozone pollution exacerbated by extreme high temperatures. *Atmos. Chem. Phys.* **2022**, *22*, 4705−4719.
(26) Gao, M.; Wang, F.; Ding, Y.; Wu, Z.; Xu, Y.; Lu, X.; Wang, Z.; Carmichael, G. R.; McElroy, M. B. Large-scale climate patterns offer preseasonal hints on the co-occurrence of heat wave and O3 pollution in China. *Proc. Natl. Acad. Sci. U.S.A.* **2023**, *120*, No. e2218274120.
(27) Lyu, X.; Li, K.; Guo, H.; Morawska, L.; Zhou, B.; Zeren, Y.; Jiang, F.; Chen, C.; Goldstein, A. H.; Xu, X.; Wang, T.; Lu, X.; Zhu, T.; Querol, X.; Chatani, S.; Latif, M. T.; Schuch, D.; Sinha, V.; Kumar, P.; Mullins, B.; Seguel, R.; Shao, M.; Xue, L.; Wang, N.; Chen, J.; Gao, J.; Chai, F.; Simpson, I.; Sinha, B.; Blake, D. R. A synergistic ozone-climate control to address emerging ozone pollution challenges. *One Earth* **2023**, *6*, 964−977.
(28) Turnock, S. T.; Smith, S. J.; Kharin, V.; Ziehn, T.; et al. Historical and future changes in air pollutants from CMIP6 models. *Atmos. Chem. Phys.* **2020**, *20* (19), 14547−14579.
(29) Xu, B.; Wang, T.; Ma, D.; Song, R.; Zhang, M.; Gao, L.; Li, S.; Zhuang, B.; Li, M.; Xie, M. Impacts of regional emission reduction and global climate change on air quality and temperature to attain carbon neutrality in China. *Atmos. Res.* **2022**, *279*, No. 106384.
(30) Vazquez Santiago, J.; Hata, H.; Martinez-Noriega, E. J.; Inoue, K. Ozone trends and their sensitivity in global megacities under the warming climate. *Nat. Commun.* **2024**, *15*, No. 10236.
(31) Fu, T. M.; Tian, H. Climate Change Penalty to Ozone Air Quality: Review of Current Understandings and Knowledge Gaps. *Curr. Pollut. Rep.* **2019**, *5*, 159−171.
(32) Weng, X.; Li, J. W.; Forster, G. L.; Nowack, P. Large modeling uncertainty in projecting decadal surface ozone changes over city clusters of China. *Geophys. Res. Lett.* **2023**, *50*, No. e2023GL103241.
(33) Griffiths, P. T.; Murray, L. T.; Zeng, G.; Shin, Y. M.; Abraham, N. L.; Archibald, A. T.; Deushi, M.; Emmons, L. K.; Galbally, I. E.; Hassler, B.; Horowitz, L. W.; Keeble, J.; Liu, J.; Moeini, O.; Naik, V.; O'Connor, F. M.; Oshima, N.; Tarasick, D.; Tilmes, S.; Turnock, S. T.; Wild, O.; Young, P. J.; Zanis, P. Tropospheric ozone in CMIP6 simulations. *Atmos. Chem. Phys.* **2021**, *21*, 4187−4218.
(34) Fiore, A. M.; Hancock, S. E.; Lamarque, J.-F.; Correa, G. P.; Chang, K.-L.; Ru, M.; Cooper, O.; Gaudel, A.; Polvani, L. M.;

https://doi.org/10.1021/acs.est.5c11992
Environ. Sci. Technol. 2026, 60, 3135−3147

Sauvage, B.; Ziemke, J. R. Understanding recent tropospheric ozone trends in the context of large internal variability: a new perspective from chemistry-climate model ensembles. *Environ. Res.: Clim.* **2022**, *1*, No. 025008.
(35) Liu, Z.; Doherty, R. M.; Wild, O.; O'Connor, F. M.; Turnock, S. T. Correcting ozone biases in a global chemistry−climate model: implications for future ozone. *Atmos. Chem. Phys.* **2022**, *22*, 12543−12557.
(36) He, S.; Yang, Y.; Wang, H.; Wang, P.; Liao, H. Source attribution of near-surface ozone pollution in Jiangsu Province of China over 2013−2019. *Atmos. Environ.* **2025**, *352*, No. 121205.
(37) Wang, Y.; Yan, Y.; Duan, K.; Kong, S.; Lin, J.; Zheng, H.; Song, A.; Zhang, Z. Effect of springtime thermal forcing over Tibetan Plateau on summertime ozone in Central China during the period 1950−2019. *Atmos. Res.* **2021**, *261*, No. 105735.
(38) Ye, X.; Wang, X.; Zhang, L. Diagnosing the Model Bias in Simulating Daily Surface Ozone Variability Using a Machine Learning Method: The Effects of Dry Deposition and Cloud Optical Depth. *Environ. Sci. Technol.* **2022**, *56*, 16665−16675.
(39) Du, J.; Qiao, F.; Lu, P.; Yu, L. Forecasting ground-level ozone concentration levels using machine learning. *Resour., Conserv. Recycl.* **2022**, *184*, No. 106380.
(40) Vairo, T.; Rapuzzi, A.; Lecca, M.; Fabiano, B. A data driven model for ozone concentration prediction in a coastal urban area. *Chem. Eng. Trans.* **2020**, *82*, 379−384.
(41) Bertrand, J.-M.; Meleux, F.; Ung, A.; Descombes, G.; Colette, A. Technical note: Improving the European air quality forecast of the Copernicus Atmosphere Monitoring Service using machine learning techniques. *Atmos. Chem. Phys.* **2023**, *23*, 5317−5333.
(42) Xiong, K.; Xie, X.; Mao, J.; Wang, K.; Huang, L.; Li, J.; Hu, J. Improving the accuracy of O3 prediction from a chemical transport model with a random forest model in the Yangtze River Delta region, China. *Environ. Pollut.* **2023**, *319*, No. 120926.
(43) O'Neill, B. C.; Tebaldi, C.; van Vuuren, D. P.; Eyring, V.; Friedlingstein, P.; Hurtt, G.; Knutti, R.; Kriegler, E.; Lamarque, J.-F.; Lowe, J.; Meehl, G. A.; Moss, R.; Riahi, K.; Sanderson, B. M. The Scenario Model Intercomparison Project (ScenarioMIP) for CMIP6. *Geosci. Model Dev.* **2016**, *9*, 3461−3482.
(44) Eyring, V.; Bony, S.; Meehl, G. A.; Senior, C. A.; Stevens, B.; Stouffer, R. J.; Taylor, K. E. Overview of the Coupled Model Intercomparison Project Phase 6 (CMIP6) Experimental Design and Organization. *Geosci. Model Dev.* **2016**, *9*, 1937−1958.
(45) Li, K.; Jacob, D. J.; Liao, H.; Qiu, Y.; Shen, L.; Zhai, S.; Bates, K. H.; Sulprizio, M. P.; Song, S.; Lu, X.; Zhang, Q.; Zheng, B.; Zhang, Y.; Zhang, J.; Lee, H. C.; Kuk, S. K. Ozone pollution in the North China Plain spreading into the late-winter haze season. *Proc. Natl. Acad. Sci. U.S.A.* **2021**, *118*, No. e2015797118.
(46) Li, K.; Jacob, D. J.; Shen, L.; Lu, X.; De Smedt, I.; Liao, H. Increases in surface ozone pollution in China from 2013 to 2019: anthropogenic and meteorological influences. *Atmos. Chem. Phys.* **2020**, *20*, 11423−11433.
(47) Emmons, L. K.; Schwantes, R. H.; Orlando, J. J.; Tyndall, G. S.; Kinnison, D. E.; Lamarque, J.-F.; Marsh, D. R.; Mills, M. J.; Tilmes, S.; Bardeen, C. A.; Buchholz, R. R.; Conley, A. J.; Gettelman, A.; Garcia, R. R.; Simpson, I.; Blake, D. R.; Meinardi, S.; Pétron, G. The Chemistry Mechanism in the Community Earth System Model Version 2 (CESM2). *J. Adv. Model. Earth Syst.* **2020**, *12* (4), No. e2019MS001882.
(48) Tilmes, S.; Hodzic, A.; Emmons, L. K.; Mills, M. J.; Gettelman, A.; Kinnison, D. E.; Park, M.; Lamarque, J. F.; Vitt, F.; Shrivastava, M.; Campuzano-Jost, P.; Jimenez, J. L.; Liu, X. Climate Forcing and Trends of Organic Aerosols in the Community Earth System Model (CESM2). *J. Adv. Model. Earth Syst.* **2019**, *11*, 745.
(49) Lin, S.-J.; Rood, R. B. An Explicit Flux-Form Semi-Lagrangian Shallow-Water Model on the Sphere. *Q. J. R. Meteorol. Soc.* **1997**, *123*, 2477−2498.
(50) Gettelman, A.; Hannay, C.; Bacmeister, J. T.; Neale, R. B.; Pendergrass, A. G.; Danabasoglu, G.; et al. High Climate Sensitivity in the Community Earth System Model Version 2 (CESM2). *Geophys. Res. Lett.* **2019**, *46*, 8329−8337.
(51) Hoesly, R. M.; Smith, S. J.; Feng, L.; Klimont, Z.; Janssens-Maenhout, G.; Pitkanen, T.; Seibert, J. J.; Linh, V.; Andres, R. J.; Bolt, R. M.; et al. Historical (1750−2014) Anthropogenic Emissions of Reactive Gases and Aerosols from the Community Emissions Data System (CEDS). *Geosci. Model Dev.* **2018**, *11*, 369−408.
(52) Feng, L.; Smith, S. J.; Braun, C.; Crippa, M.; Gidden, M. J.; Hoesly, R.; Klimont, Z.; van Marle, M.; van den Berg, M.; van der Werf, G. R. The Generation of Gridded Emissions Data for CMIP6. *Geosci. Model Dev.* **2020**, *13*, 461−482.
(53) McDuffie, E. E.; Smith, S. J.; O'Rourke, P.; Tibrewal, K.; Venkataraman, C.; Marais, E. A.; Zheng, B.; Crippa, M.; Brauer, M.; Martin, R. V. A Global Anthropogenic Emission Inventory of Atmospheric Pollutants from Sector- and Fuel-Specific Sources (1970−2017): An Application of the Community Emissions Data System (CEDS). *Earth Syst. Sci. Data* **2020**, *12*, 3413−3442.
(54) Guenther, A. B.; Jiang, X.; Heald, C. L.; Sakulyanontvittaya, T.; Duhl, T.; Emmons, L. K.; Wang, X. The Model of Emissions of Gases and Aerosols from Nature version 2.1 (MEGAN2.1): an extended and updated framework for modeling biogenic emissions. *Geosci. Model Dev.* **2012**, *5* (6), 1471−1492.
(55) Hand, R.; Keenlyside, N. S.; Omrani, N.-E.; Bader, J.; Greatbatch, R. J. The role of local sea surface temperature pattern changes in shaping climate change in the North Atlantic sector. *Clim. Dyn.* **2019**, *52*, 417−438.
(56) Liu, W.; Fedorov, A. V.; Xie, S.-P.; Hu, S. Climate impacts of a weakened Atlantic Meridional Overturning Circulation in a warming climate. *Sci. Adv.* **2020**, *6* (26), No. eaaz4876, DOI: 10.1126/sciadv.aaz4876.
(57) Jeong, Y.; Kim, S.-W.; Kim, J.; Shin, D.; Kim, J.; Park, J.-H.; An, S.-I. Influence of ENSO on Tropospheric Ozone Variability in East Asia. *J. Geophys. Res.* **2023**, *128*, No. e2023JD038604.
(58) Kim, S. W.; Kim, K. M.; Jeong, Y.; Seo, S.; Park, Y.; Kim, J. Changes in surface ozone in South Korea on diurnal to decadal timescales for the period of 2001−2021. *Atmos. Chem. Phys.* **2023**, *23*, 12867−12886.
(59) Gelaro, R.; McCarty, W.; Suárez, M. J.; Todling, R.; Molod, A.; Takacs, L.; Randles, C. A.; Darmenov, A.; Bosilovich, M. G.; Reichle, R.; Wargan, K.; Coy, L.; Cullather, R.; Draper, C.; Akella, S.; Buchard, V.; Conaty, A.; da Silva, A. M.; Gu, W.; Kim, G.-K.; Koster, R.; Lucchesi, R.; Merkova, D.; Nielsen, J. E.; Partyka, G.; Pawson, S.; Putman, W.; Rienecker, M.; Schubert, S. D.; Sienkiewicz, M.; Zhao, B. The modern-era retrospective analysis for research and applications, version 2 (MERRA-2). *J. Clim.* **2017**, *30* (14), 5419−5454.
(60) Akiba, T.; Sano, S.; Yanase, T.; Ohta, T.; Koyama, M.et al. In *Optuna: A Next-Generation Hyperparameter Optimization Framework*, Proc 25th ACM SIGKDD International Conference on Knowledge Discovery & Data Mining, 2019; pp 2623−2631.
(61) Gao, Y.; Kou, W.; Cheng, W.; Guo, X.; Qu, B.; Wu, Y.; Zhang, S.; Liao, H.; Chen, D.; Leung, L. R.; Wild, O.; Zhang, J.; Lin, G.; Su, H.; Cheng, Y.; Pöschl, U.; Pozzer, A.; Zhang, L.; Lamarque, J.-F.; Guenther, A. B.; Brasseur, G.; Liu, Z.; Lu, H.; Li, C.; Zhao, B.; Wang, S.; Huang, X.; Pan, J.; Liu, G.; Liu, X.; Lin, H.; Zhao, Y.; Zhao, C.; Meng, J.; Yao, X.; Gao, H.; Wu, L. Reducing long-standing surface ozone overestimation in Earth system modeling by high-resolution simulation and dry deposition improvement. *J. Adv. Model. Earth Syst.* **2025**, *17*, No. e2023MS004192.
(62) Ding, A.; Wang, T.; Zhao, M.; Wang, T.; Li, Z. Simulation of Sea-Land Breezes and a Discussion of Their Implications on the Transport of Air Pollution during a Multi-Day Ozone Episode in the Pearl River Delta of China. *Atmos. Environ.* **2004**, *38*, 6737−6750.
(63) Wang, T.; Xue, L.; Brimblecombe, P.; Lam, Y. F.; Li, L.; Zhang, L. Ozone Pollution in China: A Review of Concentrations, Meteorological Influences, Chemical Precursors, and Effects. *Sci. Total Environ.* **2017**, *575*, 1582−1596.
(64) Lu, X.; Hong, J.; Zhang, L.; Cooper, O. R.; Schultz, M. G.; Xu, X.; Wang, T.; Gao, M.; Zhao, Y.; Zhang, Y. Severe Surface Ozone

Pollution in China: A Global Perspective. *Environ. Sci. Technol. Lett.* **2018**, *5*, 487−494.
(65) Li, H.; Yang, Y.; Jin, J.; Wang, H.; Li, K.; Wang, P.; Liao, H. Climate-driven deterioration of future ozone pollution in Asia predicted by machine learning with multi-source data. *Atmos. Chem. Phys.* **2023**, *23*, 1131−1145.
(66) Li, H.; Yang, Y.; Su, H.; Wang, H.; Wang, P.; Liao, H. Ozone pollution in China affected by climate change in a carbon neutral future as predicted by a process-based interpretable machine learning method. *Geophys. Res. Lett.* **2024**, *51*, No. e2024GL109520.
(67) Zanis, P.; Akritidis, D.; Turnock, S.; Naik, V.; Szopa, S.; Georgoulias, A. K.; Bauer, S. E.; Deushi, M.; Horowitz, L. W.; Keeble, J.; Le Sager, P.; O'Connor, F. M.; Oshima, N.; Tsigaridis, K.; Van Noije, T. Climate change penalty and benefit on surface ozone: a global perspective based on CMIP6 earth system models. *Environ. Res. Lett.* **2022**, *17*, No. 024014.
(68) Kang, L.; Liao, H.; Li, K.; Yue, X.; Yang, Y.; Wang, Y. Effects of 2010−2045 climate change on ozone levels in China under a carbon neutrality scenario: key meteorological parameters and processes. *Atmos. Chem. Phys.* **2025**, *25*, 3603−3621.
(69) Young, P. J.; Archibald, A. T.; Bowman, K. W.; Lamarque, J.-F.; Naik, V.; Stevenson, D. S.; Tilmes, S.; Voulgarakis, A.; Wild, O.; Bergmann, D.; Cameron-Smith, P.; Cionni, I.; Collins, W. J.; Dalsøren, S. B.; Doherty, R. M.; Eyring, V.; Faluvegi, G.; Horowitz, L. W.; Josse, B.; Lee, Y. H.; MacKenzie, I. A.; Nagashima, T.; Plummer, D. A.; Righi, M.; Rumbold, S. T.; Skeie, R. B.; Shindell, D. T.; Strode, S. A.; Sudo, K.; Szopa, S.; Zeng, G. Pre-industrial to end 21st century projections of tropospheric ozone from the Atmospheric Chemistry and Climate Model Intercomparison Project (ACCMIP). *Atmos. Chem. Phys.* **2013**, *13* (4), 2063−2090.
(70) Fang, T.; Hu, J.; Gu, Y.; Sung, J. J. Y.; Yim, S. H. L. Response of ozone to current and future emission scenarios and the resultant human health impact in Southeast Asia. *Environ. Int.* **2025**, *197*, No. 109333.
(71) Yang, J.; Wang, Y.; Zhang, L.; Zhao, Y. Investigating the response of China's surface ozone concentration to the future changes of multiple factors. *Atmos. Chem. Phys.* **2025**, *25*, 2649−2666.
(72) Hansen, J.; Sato, M.; Kharecha, P.; von Schuckmann, K. Earth's Energy Imbalance and Implications. *Atmos. Chem. Phys.* **2011**, *11*, 13421−13449.

https://doi.org/10.1021/acs.est.5c11992
Environ. Sci. Technol. 2026, 60, 3135−3147